

# **Targeted mutational analysis to unravel the complexity of African horse sickness virus NS3 function in mammalian cells**

Authors: Linda Ferreira-Venter<sup>a</sup>, Eudri Venter<sup>b</sup>, Jacques Theron<sup>a</sup>, Vida van Staden<sup>a</sup>

Affiliations/ author addresses:

- a. Department of Biochemistry, Genetics and Microbiology, University of Pretoria, Pretoria 0002, South Africa.
- b. Laboratory for Microscopy and Microanalysis, University of Pretoria, Pretoria 0002, South Africa

Corresponding author:

Vida van Staden

vida.vanstaden@up.ac.za

Tel: +270124203257

Fax: +27123625327

Present address:

Department of Biochemistry, Genetics and Microbiology, University of Pretoria, Private Bag X20, Hatfield, 002, Pretoria, South Africa

Declarations of interest: none.

## **Abstract**

The African horse sickness virus non-structural protein 3 (NS3) is involved in the final stages of infection. To gain insight into the function of different NS3 domains, we generated reverse genetics-derived mutants, each expressing a modified version of the protein. A functional comparison of these mutants to the wild-type virus in mammalian cells indicated the variable contribution of the different domains to the cytopathic effect and in ensuring effective virus trafficking and release. The transmembrane domains were determined as essential mediators of NS3 localisation, as the abnormal processing of these mutant proteins resulted in their nuclear localisation and interaction with NS1. NS3 cytoplasmic domain disruptions resulted in increased cytosolic virus particle accumulation and abnormal virion tethering to plasma membranes. Other aspects of infection were also affected, such as VIB formation and distribution of the outer capsid proteins. Overall, these results illustrate the intricate role of NS3 in the infection cycle.

## **Key Words**

AHSV

NS3

Reverse genetics

Virus trafficking

Virus release

NS1

Protein functional domains

## Introduction

African horse sickness (AHS) is a highly infectious, often fatal disease of equids, endemic to sub-Saharan Africa (Mellor and Hamblin, 2004) and listed as a notifiable disease by the World Organization for Animal Health (OIE). With its high lethality and ability to rapidly spread, the disease causes a significant economic burden, with the loss of animals and trade restrictions (Zientara et al., 2015). The etiological agent of the disease is African horse sickness virus (AHSV), a member of the *Reoviridae* family. As a non-contagious disease, the virus is exclusively transmitted by its vector the *Culicoides* biting midge (Du Toit, 1944; Venter et al., 2009).

Similar to other orbiviruses, the AHSV virion consists of a non-enveloped triple-layered icosahedral particle, enclosing ten double stranded RNA molecules (Manole et al., 2012). These RNA segments encode for seven structural proteins (VP1-VP7) constituting the virus particle and transcription complexes, and four non-structural proteins (NS1, NS2, NS3/A and NS4) only produced upon infection (Bremer et al., 1990; Zwart et al., 2015). The non-structural proteins appear to have mostly supportive roles, providing the virus with a replicative advantage (Owens et al., 2004; Van Gennip et al., 2014).

Of all the non-structural proteins, NS3 has the most diverse repertoire of functions in the viral infection cycle. These include mediating intracellular virus trafficking and release and down-regulation of the host cell's innate immune response (Beaton et al., 2002; Bhattacharya et al., 2015; Celma and Roy, 2009, 2011; Chauveau et al., 2013). AHSV NS3 was previously identified as a key protein in mediating virus release and membrane permeability (Meiring et al., 2009). Through sequence comparisons various functional domains have been identified for the AHSV and bluetongue virus (BTV) NS3 proteins. AHSV Seg-10 contains two in-frame start codons allowing equi-molar expression of the full-length NS3 and its truncated version, NS3A (van Staden and Huismans, 1991). With the successful rescue of knockout mutants no longer expressing either one or both proteins, it has been shown that in the case of BTV, the NS3/A proteins are non-essential to virus replication. However, it has been proposed that NS3A might play an additional as yet unidentified role in insect cells (Feenstra et al., 2014; van de Water et al., 2015; Van Gennip et al., 2014). Recently an overlapping +1 open reading frame (ORF) was identified in both BTV and AHSV Seg-10, but the exact function of the encoded protein remains unclear (Sealfon et al., 2015; Stewart et al., 2015).

As an arbovirus, AHSV is able to successfully propagate in both the mammalian host and the insect vector. However NS3 expression levels, and the mechanism whereby it mediates virus particle release, appear to be differentially regulated in the two cell types. In mammalian cells virus release is primarily via a passive lytic process, while it is non-lytic in insect cells (Venter et al., 2014). Possibly contributing to the cytopathogenicity observed in mammalian cells, the integral membrane protein NS3/A functions as a viroporin that modifies membrane permeability (Han and Harty, 2004; van Niekerk et al., 2001; van Staden et al., 1995). The two hydrophobic transmembrane (TM) domains of NS3/A have been linked to its cytotoxic activity. Disruption of either of the TM domains prohibits its normal transport and association with cellular membranes, resulting in a marked decrease in cytopathic effect (CPE) (van de Water et al., 2015; van Niekerk et al., 2001).

Non-lytic release from mammalian cells has also been observed for both AHSV and BTV (Celma and Roy, 2009; Venter et al., 2014). This might be mediated by the interaction of late assembly domain (LD) motifs in the cytoplasmic N-terminus of NS3/A with components of the cellular ESCRT (Endosomal Sorting Complex Required for Transport) machinery (Celma and Roy, 2009; Van Gennip et al., 2014; Wirblich et al., 2006). AHSV and BTV NS3/A encode for two different types of LD motifs, namely P(T/S)AP and PPXnY (Bhattacharya et al., 2015). Both of these act as separate entry points into the ESCRT pathway. The P(S/T)AP motif is recognised by the ESCRT-I component Tsg-101 (Garrus et al., 2001), while the PPXnY motif is recognised by NEDD4 ubiquitin ligases ensuring ubiquitination and subsequent recruitment by ubiquitin-binding components of the ESCRT pathway (Ingham et al., 2004). Disruption of the BTV LD motifs resulted in abnormal virus localisation and release, with the virus particles remaining tethered to the cellular membrane (Bhattacharya et al., 2015; Wirblich et al., 2006). None of these LD motifs have been investigated in detail for AHSV.

It has also not yet been established how AHSV NS3 interacts with the mature virus particle. In BTV the C-terminus of NS3/A associates with the outermost virus particle protein VP2, facilitating the virus's trafficking and release from the cell (Beaton et al., 2002; Celma and Roy, 2009).

A wealth of information is available for BTV NS3, while investigation on the cognate AHSV protein has lagged behind. AHSV is distinctly dissimilar to BTV in many key aspects, including its host range, disease progression, virulence factors and degree of inter-strain gene segment sequence conservation. Therefore,

while inferences about the role of AHSV NS3 can be made based on results obtained from BTV, the inherent differences between these two species justify a separate investigation on the AHSV NS3 protein.

Here we attempt to improve our understanding of the function of NS3/A in the final stages of AHSV morphogenesis in mammalian cells. We describe the reverse genetics-based generation and subsequent comparative characterisation of seven AHSV-4 (serotype 4) mutants, each expressing a modified version of NS3/A. Our results show that disruption of any of the NS3/A functional domains resulted in reduced virus release and CPE. We identified the transmembrane domains as the main determinants required for the optimal functioning of the protein, essential to its proper processing and distribution within the cell. Also, AHSV potentially utilises the ESCRT pathway to facilitate trafficking and release. Mutating NS3/A also influenced the localisation and/or function of multiple other structural and non-structural viral proteins. Ultimately, we gained insight into the contribution of the different domains of NS3/A in allowing the proteins to achieve their various functions in the cell.

## Results

### *Rescue of seven NS3/A mutant AHS viruses*

To investigate the importance of different NS3 domains in the virus infection cycle, reverse genetics was used to generate a number of mutant AHSV-4 strains, each expressing a modified version of the NS3 protein (Fig. 1A). The proposed amino acid changes were based on previous work done for BTV and AHSV, where it was shown that the introduced mutations were sufficient to disrupt the normal function of the targeted region (Bhattacharya et al., 2015; Celma and Roy, 2009; Celma and Roy, 2011; Van Gennip et al., 2014; van Niekerk et al., 2001; Wirblich et al., 2006). Of interest for this study was the NS3 and NS3A start codons (STR1 and STR2), the late-domain motifs (LD1 and LD2), the transmembrane domains (TM1 and TM2) and the C-terminal region (CTD) of the protein.

For mutant virus rescue, a plasmid-based reverse genetics approach was used (Conradie et al., 2016). Nine mutant Seg-10 constructs were generated and used in combination with plasmids encoding the other nine unmodified gene segments. Virus rescue from all nine transfections was confirmed by the appearance of CPE and isolation of dsRNA from harvested cells (results not shown). PCR amplification and sequencing of Seg-10 however revealed that only AHSV4\_STR2, AHSV4\_LD1, AHSV4\_LD2, AHSV4\_TM1, AHSV4\_TM2, AHSV4\_TM1&2 and AHSV4\_CTD contained the desired point mutations. AHSV4\_STR1 and AHSV4\_NULL showed reversion, with the introduced 'GC' point mutations at nucleotide position 1 and 2 of the first start codon changing back to the original 'AT'. These transfections were repeated at least twice, with the rescued viruses consistently re-establishing this start codon within one to two passages in tissue culture. Interestingly, for AHSV\_NULL the mutated second start codon did not revert back. With the perceived inability to rescue a mutant no longer expressing the full-length NS3, we proceeded to characterise the remaining seven mutants.

The stability of all introduced point mutations was confirmed for at least five passages in tissue culture. We also established by Western blot that all mutants expressed their respective NS3/A proteins (Fig. 1B). Two bands, approximately 1 kDa apart, were observed for all of the viruses except AHSV4\_STR2. As expected, this mutant expressed only the larger  $\pm 23$  kDa NS3 protein, indicating the successful disruption of its NS3A start codon. The results also confirmed the successful 19 amino acid deletion from the C-terminal end of

AHSV4\_CTD NS3 and NS3A, their smaller sizes approximately 20 kDa and 19 kDa respectively. To assess the impact of the introduced mutations on the solubility of the protein, whole cell lysates were subjected to a solubility assay and Western blot (Fig. 1B). The NS3/A proteins of AHSV4\_WT, AHSV4\_STR2, AHSV4\_LD1, AHSV4\_LD2 and AHSV4\_CTD were fully insoluble, as expected of an integral membrane protein. NS3/A from AHSV4\_TM1, AHSV4\_TM2 and AHSV4\_TM1&2 however also had a minor soluble component, probably due to their reduced hydrophobicity and inability to stably interact with membranes (van Niekerk et al., 2001).

#### *Comparison of virus release and cytopathogenicity of wild-type and mutant strains*

As an initial assessment of the ability of the different viruses to replicate and spread, their plaque forming abilities in BSR cells were compared (Fig. 2A). AHSV4\_STR2 formed plaques similar to those of the wild-type virus, with mostly larger foci of cell death. In contrast to this, the plaques of AHSV4\_LD1 and AHSV4\_LD2 were notably and consistently smaller. Furthermore none of the AHSV4\_TM mutants or AHSV4\_CTD formed distinct plaques, but cell death was present with faint regions of discolouration, interspersed with unaffected areas of viable cells. Immunoperoxidase monolayer assays (IPMA; immunostaining with an anti-NS2 antibody and peroxidase-conjugated Protein A) of infected BSR and Vero cells confirmed that viral replication was taking place for the AHSV4\_TM mutants and AHSV4\_CTD (Fig. 2B). The lack of observable plaques in these cases therefore indicated a putative disruption of normal efficient virus release.

We subsequently compared the percentage virus released by the different virus strains. Viral titres in the culture medium and the cells respectively were determined at different times post infection, using a combination of TCID<sub>50</sub> and IPMA (immunostaining with an anti-NS2 and Alexa Fluor<sup>TM</sup> 488 antibodies). While none of the NS3 modifications adversely affected virus yield (Supplementary Fig. S1), the absence of functional LD motifs, TM domains or the C-terminal region of the protein, appeared to prevent effective virus release (Fig. 3A). Apart from AHSV4\_STR2, all of the mutants showed less than 1% release up to 24 h p.i. and less than 18% release up to 72 h p.i.. In contrast to this, the wildtype virus exhibited over 9% release

at 12 h p.i. and over 40% release at the later time points. AHSV4\_STR2 showed similar release to AHSV4\_WT at 24-72 h p.i., but significantly higher release at the early time point of 12 h p.i..

The plaque and IPMA assays indicated that disruption of any one of a number of NS3 domains might influence the virus's ability to cause cell death. These results were supported by a cytotoxicity assay (Fig. 3B), with the most prominent differences in cell viability observed from 24-72 h p.i.. AHSV4\_WT and AHSV4\_STR2 resulted in similar CPE, with a marked decrease ( $\pm 90\%$ ) in live cells over this period. This high cell death could contribute to the relative lower levels of the NS3\_WT and NS3\_STR2 protein expression observed in Fig. 1B. Cells infected with AHSV4\_TM1, AHSV4\_TM2, AHSV4\_TM1&2 and AHSV4\_CTD remained mostly viable up to 48 h p.i., with a subsequent  $\pm 40\%$  reduction in live cells by 72 h p.i.. AHSV4\_LD1 and AHSV4\_LD2 showed a CPE phenotype intermediate to these two classes. The sustained viability of cells infected by all of these mutants could allow for the higher intracellular accumulation of the NS3 proteins as observed by the Western blots (Fig. 1B).

Taken together it was clear that the different NS3/A domain disruptions had resulted in distinct mutant virus phenotypes, variable with regards to plaque morphology, virus release and cytopathogenicity.

#### *Characterisation of the intracellular localisation of the wild-type and mutant NS3/A proteins*

To gain insight into the underlying causes of the observed mutant phenotypes, we investigated the intracellular distribution of NS3 for each virus by confocal laser scanning microscopy (CLSM). AHSV4\_STR2, AHSV4\_LD1, AHSV4\_LD2 and AHSV4\_CTD exhibited a pattern essentially indistinguishable from that of the wild-type virus, with distinct perinuclear and plasma membrane localisation of NS3 (Fig. 4). Unexpectedly, AHSV4\_TM1 and AHSV4\_TM1&2 showed a mixed cytoplasmic and predominantly intranuclear distribution of NS3/A, with the NS3 signal being either diffuse, or foci, or distributed as bundles of thin fibres. While AHSV4\_TM2 also occasionally exhibited this intranuclear localisation, the protein's distribution was generally more diffuse cytoplasmic and perinuclear. The true intranuclear presence of these NS3 proteins was confirmed with Z-stack analyses and orthogonal sectioning (results not shown). Sequence analysis indicated that our amino acid substitutions had not introduced classical nuclear localisation signal (NLS) sequences to the mutant TM proteins.



The nuclear localisation of the TM mutant proteins was further confirmed with TEM visualisation. Wild-type NS3 showed strong labelling to the plasma membrane and perinuclear vesicles (Fig. 5), with the same distribution pattern observed for AHSV4\_STR2, AHSV4\_LD1, AHSV4\_LD2 and AHSV4\_CTD (not shown). NS3 of the TM mutants however showed specific labelling to the nucleus and what appeared to be viral tubules (Fig. 5). Immunogold labelling with an anti-NS1 antibody confirmed that these tubules were NS1 in origin (Fig. 5 insert). This association between the TM mutant NS3 proteins and NS1 was further confirmed using CLSM and dual immunolabelling (Fig. 6). While there was no detectable co-localisation with NS1 for the wild-type NS3 (Pearson's R value of  $-0.13 \pm 0.078$ ), the mutant proteins only appeared as thin fibres in areas with NS1 overlap (Pearson's R value of  $0.616 \pm 0.077$ ) indicating a relatively strong correlation (Dunn et al., 2011). This association was not detected for any of the other mutant proteins.

Overall these results illustrate the importance of the transmembrane domains in ensuring the proper processing and distribution of the NS3/A proteins once synthesised. However, while the NS3/A proteins of the LD and CTD mutants localised normally, virus release and spread was still affected, indicating specific disruption of key interactions with cellular proteins and/or virions.

#### *Assessing the importance of the different NS3/A domains in virus morphogenesis*

To further investigate how the different NS3/A domain disruptions contribute to the observed mutant phenotypes, we assessed the overall distribution of mature virus particles in infected mammalian cells by CLSM using an antibody specific to the outer capsid protein VP2 (Fig. 7). The VP2 profiles of AHSV4\_STR2 and AHSV4\_WT were similar, showing predominantly small cytoplasmic foci. In contrast to this, AHSV4\_LD1 and AHSV4\_LD2 showed prevalent VP2 membrane localisation, with limited cytoplasmic foci. The TM mutants all exhibited large cytoplasmic foci, while AHSV4\_CTD appeared intermediate with both VP2 foci and plasma membrane interaction. The distribution pattern of VP5, the other outer capsid protein, was nearly identical to that of VP2 for all of the virus strains, except that some minimal membrane localisation of VP5 was also detected in cells infected with the transmembrane mutants (Supplementary Fig. S2). While no clear co-localisation could be detected between NS3 and either VP2 or

VP5 for any of the virus strains, the different NS3/A modifications appeared to impact virus particle localisation.

For a more in-depth analysis of virus morphogenesis, the different strains were compared on an ultrastructural level by electron microscopy. While the synthesis and distribution of virus-encoded VP7 crystals and NS1 tubules remained unchanged in all cases, marked differences were observed in the localisation of the virus particles within the infected cells (Fig. 8), corresponding to the VP2 and VP5 CLSM data. In the case of AHSV4\_WT, AHSV4\_STR2, AHSV4\_LD1 and AHSV4\_LD2, virus particles were present throughout the cytoplasm and as small virus aggregates (<20 virus particles). In contrast to this, AHSV4\_TM1, AHSV4\_TM2, AHSV4\_TM1&2 and AHSV4\_CTD formed large cytoplasmic virus aggregates (average of 20-90 virus particles) in infected cells. The reduced virus release observed with these mutants therefore appeared to be due to a lack of transport of newly formed virions, with their preferential accumulation in the cytoplasm. While AHSV4\_LD1 and AHSV4\_LD2 did not form large aggregates they also exhibited a unique mutant phenotype, with virus particles tethered to the plasma membrane (Fig. 8). Therefore, while in these mutants particles were successfully trafficked from their sites of synthesis without cytoplasmic accumulation, their release was still defective at the plasma membrane.

It was noted that in certain instances the virus aggregates were in close proximity to VIBs (Fig 9). This was supported by CLSM, with the presence of VP2 or VP5 foci adjacent to/surrounding VIBs (Supplementary Fig. S3). These observations were sufficiently frequent to let us speculate as to whether the NS3/A mutations, and their resultant disruption of virus particle transport and release, could also affect other aspects of the virus infection cycle. From the TEM data it appeared as though infection by some of the mutants (e.g. AHSV4\_TM2) resulted in the production of larger VIBs compared to the wild-type virus. As the micrographs could not provide an accurate assessment of overall VIB size and distribution in infected cells, we proceeded with CLSM of infected cells labelled with an anti-NS2 antibody (Fig. 9; Supplementary Fig. S4). There were obvious size differences in the VIBs of cells infected with the different mutant strains. To quantify these differences, we used ImageJ and assessed Maximum Intensity Projection (MIP) images, measuring the approximate size of each VIB in 20 infected cells for all virus strains (Fig. 9). These results showed that smaller VIBs, between  $0.1 - 2.0 \mu\text{m}^2$ , were prevalent at 24 h p.i. for all of the viruses. However, the proportion of larger VIBs ( $2.0 - 20+ \mu\text{m}^2$ ) was increased for the LD, TM and CTD mutants. It therefore

appeared as though larger VIBs formed as a result of cytoplasmic virion accumulation and ineffective virus particle trafficking and release.

## **Discussion**

Several functions have been linked to NS3, and its truncated version NS3A, in the orbivirus infection cycle. As non-structural proteins, their expression is only detected upon infection, where their association with mature virions, the cell membrane, as well as cellular transport and exocytotic machinery have implicated them in mediating trafficking and release of virus particles from the cell. Most of these studies involved BTV NS3/A, with a limited number of investigations on the cognate AHSV protein. This study therefore aimed, through the generation and analysis of recombinant viruses expressing modified Seg-10 genes, to clarify and improve our understanding of the role of this integral membrane protein in the AHSV infection cycle.

To correlate the activity of the various NS3/A functional domains to different aspects of the infection cycle, these regions were altered through the introduction of specific Seg-10 mutations, followed by the rescue of seven AHSV-4 NS3/A mutants using a plasmid-based reverse genetics system (Conradie et al., 2016). All of the resulting viruses exhibited unique phenotypes in comparison to the wild-type virus. One should however keep in mind that amino acid substitution mutations, as engineered here, can either directly result in abolishing specific protein-protein interactions involving those residues, or alternatively impact on the structure or folding of the protein thereby impairing the functionality of the domain.

Transfections with plasmids where the NS3 start codon was abolished resulted in virus recovery, but the introduced point mutations showed reversion and we were unable to generate a stable mutant virus not expressing the full length NS3 protein. The consistent re-establishment of this start codon was surprising, as others have managed to generate this type of BTV and AHSV mutant (Celma and Roy, 2011; van de Water et al., 2015; Van Gennip et al., 2014). It is likely that our construct was insufficient, indicating that for AHSV at least, greater disruption at the terminal end is required, whether through the insertion of additional stop codons (van de Water et al., 2015; van Rijn et al., 2018) or deletions that do not affect Seg-10's proposed role in structural motif formation and packaging (Burkhardt et al., 2014; Feenstra et al., 2014).

The second start codon did not appear to be under the same selection pressure, with the successful rescue of AHSV4\_STR2. The behaviour of this mutant in mammalian cells was nearly indistinguishable from that of the wildtype virus with respect to the ability to induce CPE or influence the distribution of other viral proteins or virions within infected cells. However, the absence of NS3A resulted in a significant increase in early virus release. Therefore the activity of the full-length NS3 protein alone appears sufficient in mediating effective virus propagation and spread in mammalian cells and could explain the apparent selection pressure for its continued expression. This however does not exclude a potentially unique role for NS3A in insect cells.

As an integral membrane protein, NS3 is trafficked via the secretory pathway. Following its synthesis at the endoplasmic reticulum (ER), NS3 is processed and inserted into lipid bilayers as it moves through the trans-Golgi network (TGN) (Evans and Graham, 1989; Lodish et al., 2000). Its folding is probably mediated from its N-terminus, with the first transmembrane domain (TM1) acting as a signal anchor sequence and the second (TM2) as a stop transfer sequence. This anchors NS3 in the membrane, with both its N- and C-termini facing the cytosol, allowing NS3 to interact with host and viral components (Lodish et al., 2004; van Staden et al., 1995; Wu et al., 1992). Through this pathway NS3 will subsequently gain access to the plasma membrane, endosomes and multivesicular bodies.

Both intact TM domains were shown to be essential for mediating the proper functional conformation of NS3 required for cellular and viral protein interactions that would normally mediate virus particle trafficking to sites of release. When one or both of the transmembrane regions were selectively disrupted, various aspects of the AHSV infection cycle were altered. Firstly, all of the AHSV\_TM mutants showed delayed CPE following infection. While similar results were obtained with previous studies based on single protein expression systems for NS3 (Han and Harty, 2004; van Niekerk et al., 2001), these are novel observations in the context of an AHSV infection. All AHSV4\_TM mutants also showed large cytoplasmic aggregates of virions, and significantly reduced virus release.

For all three AHSV\_TM mutants, the NS3 proteins did not appear to have any membrane association. As these proteins remained predominantly insoluble, one would not expect their diffuse distribution throughout the cytoplasm. AHSV4\_TM1 and AHSV4\_TM1&2 however displayed the unusual intranuclear localisation of NS3/A, for which the exact reason remains unknown. Without functional TM domain(s) these mutant

NS3/A proteins would not be properly inserted into the lipid bi-layer during their synthesis and could therefore passively also localise to the nucleus, as their small size is below the nuclear diffusion limit (Macara, 2001; Wang and Brattain, 2007). This has been proposed for NS4, where its small size and/or specific trafficking mechanisms result in its punctate or diffuse localisation patterns in both the cytoplasm and nucleus (Belhouchet et al., 2011; Ratiner et al., 2011; Zwart et al., 2015). Whether a similar mechanism is responsible for the nuclear localisation of the mutant NS3 proteins still remains to be investigated, and its distribution profile in the cytoplasm and nucleus could be due to uncharacterised interactions with cellular or viral proteins.

Interestingly, with the abnormal localisation of the NS3\_TM proteins we also showed their association with NS1 tubules. An interaction between NS3 and NS1 has been proposed for BTV, where their relative levels of expression in mammalian and insect cells were hypothesized to influence the mode of release (Owens et al., 2004). This has not yet been investigated for AHSV, and our results are the first indication of a possible interaction between these two AHSV proteins. We however only observed this interaction between NS3\_TM mutants and NS1, and not for NS3\_WT. While it has been proposed that BTV NS1 might function as a regulator of viral protein synthesis (Boyce et al., 2012), a possible related role might be as a regulator of misfolded viral proteins. The presence of NS1 tubules in the nucleus of AHSV-infected cells has been documented previously (Venter et al., 2014), however whether the tubules are assembled in or transported to the nucleus, and function (if any) there, remains to be investigated.

Ineffective virus trafficking and release did not only result from the improper processing of NS3/A, as illustrated by the release phenotypes of the three mutants AHSV4\_LD1, AHSV4\_LD2 and AHSV4\_CTD. The localisation of these strains' NS3/A proteins was similar to that of the wild-type virus, however, all these mutants showed significantly reduced virus release during infection. This is likely due to the disruption of key functional regions required for association with cellular or viral components.

The interaction between the C-terminal region of NS3 and the outer capsid protein VP2 has only been confirmed for BTV (Beaton et al., 2002; Celma and Roy, 2009). Mammalian cells infected with our AHSV4\_CTD mutant showed the aggregation of virus particles in the cytoplasm, therefore the absence of 19 amino acids from the C-terminal end of the AHSV4 NS3/A also disrupted virus particle trafficking.

AHSV4\_LD1 and AHSV4\_LD2 did not exhibit cytoplasmic virus particle accumulation to the extent of the TM domain and CTD mutants. Rather, ultrastructural analysis revealed virus particles tethered to the plasma membrane with their final release impaired, similar to what has been described for BTV (Bhattacharya et al., 2015; Celma and Roy, 2009). Research on enveloped viruses such as HIV (human immunodeficiency virus), HTLV (human T-cell leukaemia virus) and RSV (Rous sarcoma virus) have clearly illustrated the complexity of LD motifs. Often they function autonomously, exhibiting non-redundant and sequential functions (Blot et al., 2004; Bouamr et al., 2003); or they can function synergistically to ensure effective release (Strack et al., 2002; Usami et al., 2009). One LD motif might even be primarily responsible for release, with the other simply auxiliary in its function (Parent et al., 1995; Vana et al., 2004).

Our results indicate a system where the function of both AHSV LD motifs are required for effective release, as the disruption of either motif results in virion-membrane tethering. Intracellular virus trafficking does not appear to be compromised, with particles transported from their sites of synthesis to the plasma membrane. Overall these results indicate that AHSV utilises the ESCRT pathway to mediate release during infection. This corresponds to a recent study where the absence of 77 amino acids from NS3/A, including the entire late-domain, resulted in only localised viral replication of AHSV in animals vaccinated with this NS3 mutant (van Rijn et al., 2018).

Several of our introduced NS3/A mutations resulted in an altered distribution of VP2 and VP5. While their distribution patterns provide an indication of virion localisation, virus particles cannot necessarily account for all the signal observed. It is likely that when NS3/A is not functioning properly in the final stages of virus morphogenesis, this could lead to the aberrant localisation of these outer capsid proteins to the plasma membrane, in particular when considering the intrinsic membrane binding ability of VP5 (Bhattacharya and Roy, 2008; Stassen et al., 2011; Zhang et al., 2010). Although co-localisation of NS3/A with VP2 and VP5 has been observed for BTV (Beaton et al., 2002; Bhattacharya and Roy, 2008), we could not show this for AHSV. Irrespective of this, the modification of NS3/A resulted in the changed distribution of the outer capsid proteins, and therefore implies some interaction, whether direct or indirect. The possibility of lipid rafts also playing a role in AHSV morphogenesis should be considered, taking into account that NS3/A and lipid rafts are synthesised and processed within the Golgi en route to the plasma membrane (Brown and

London, 1998; Lodish et al., 2004; Parr et al., 2006); and that BTV VP5 has been shown to interact with these cholesterol enriched microdomains (Bhattacharya and Roy, 2008).

The disruptive effect of the various domain modifications on virus trafficking and release is reflected in the aberrant formation of smaller plaques by the LD mutants, as well as the complete absence of plaque formation by the TM and CTD virus strains. These results also illustrate that the induction of CPE is not only dependent on the presence of intact TM domains. All of the mutants (except AHSV4\_STR2) showed variable delayed levels of CPE compared to the wild-type virus. Considering the contribution of virus release to overall observed cell death, and the disruption of virus release in these mutants, it is suspected that the activation of cellular apoptosis by virus infection might be one of the main contributors to the ultimate death of the cells (Stassen et al., 2012; Vermaak and Theron, 2015). The eventual release of these mutants could therefore be passive, facilitated by the cell's loss of integrity and disintegration of the plasma membrane, eventually allowing the viruses to spread to other cells.

Virus yield was not significantly reduced by any of the NS3/A mutations. This indicates that aspects of virus replication, such as assembly, appeared unaffected by the ineffective transport and release of the virus particles. However, a greater proportion of large VIBs were observed for most of the mutants. The significance of this is unknown. As the largest VIBs were observed with those mutants showing cytoplasmic virion accumulation, it is possible that the absence of active virus transport in the cell, from their sites of synthesis, might actually affect the maturation of these structures. The larger VIBs might also simply be a representation of the variable effect of the different mutants on the overall biochemistry of the cell following infection.

Overall our results illustrate a complexity of domain functions for facilitating NS3 pleiotropy. Also, due to the modified function of the mutant NS3 proteins, we could highlight the interconnectedness of the infection system, with the detection of novel viral protein interactions, altered capsid protein distribution and increased VIB sizes. Further investigation is required, to elucidate the interaction between NS3 and other viral and cellular components. It will also be interesting to determine whether similar phenotypes are detected within insect cells, and whether any of the domains might exhibit a unique function. Ultimately this study emphasises the large number of questions that remain regarding the infection strategy of AHSV. As NS3/A is an ideal candidate for the development of DISA and DIVA compliant vaccines, a deeper understanding of

the virus and its infection in both the host and vector will allow for the development of improved preventative and curative strategies against the devastating disease AHS.

## **Materials and methods**

### *Cells and viruses*

Vero (ATCC CCL-81), BSR (a clone of BHK-21 cells) and BSR-T7 (Buchholz et al., 1999) (obtained from Dr Christiaan Potgieter, Deltamune) cells were maintained in monolayers in Minimal Essential Medium (MEM; Lonza), supplemented with Earle's balanced salt solution (EBSS), 5% fetal bovine serum (FBS, Gibco®), non-essential amino acids (NEAA, Lonza), antibiotics and antifungals (penicillin, streptomycin and fungizone) (Highveld Biological). Additionally, 1 mg/ml Geneticin (Invitrogen) was added to every second passage of the BSR-T7 cells. All cell lines were grown at 37°C in the presence of 5% CO<sub>2</sub>.

AHSV serotype 4 (AHSV-4) was used for this study. The origin of this live-attenuated vaccine strain has previously been described (HS32/62 10S-10BHK-3LP-5Vero) (Erasmus, 1974; van de Water et al., 2015). All of the reverse genetics generated NS3 mutant viruses had the AHSV-4 backbone (Genbank KM820849-KM820858). Stocks for all viruses were generated in BSR cells and stored at 4°C.

BSR monolayers were infected with the wild-type AHSV-4 or any of its derived NS3 mutants at the desired MOI. After allowing virus adsorptions at 37°C for 1-1.5 hours the inoculum was removed, monolayers washed twice with serum-free EMEM and then incubated in complete EMEM at 37°C with 5% CO<sub>2</sub>.

Plaque-forming ability of virus strains was determined as previously described (Oellermann, 1970). For visualisation, cells were stained with 0.1% MTT (thiazolyl blue tetrazolium bromide [Sigma Aldrich]) and incubated overnight. Viral titres were determined by endpoint dilution and expressed as TCID<sub>50</sub>/ml (50% tissue culture infective dose per millilitre).



### *Construction of modified pJAD-S10 plasmids*

Two different cloning strategies were followed depending on the number of nucleotide changes required for the different NS3/A modifications. A plasmid vector pJAD-S10 (from Dr Liesel Stassen, University of Pretoria), containing a cDNA copy of Seg-10 of the AHSV-4 genome (GenBank KM820858) was used as template (Conradie et al., 2016).

The mutant pJAD.STR1, pJAD.STR2, pJAD.NULL, pJAD.LD1 and pJAD.LD2 plasmid constructs were generated using the QuickChange<sup>®</sup> II XL site-directed mutagenesis kit (Stratagene) according to the manufacturer's specifications. For all modifications except pJAD.NULL, the pJAD-S10 was used as template along with the respective forward and reverse primers (IDT) (Supplementary Table 1). pJAD.NULL was generated using pJAD.STR2 as template with the STR1 primer set. All cloning and plasmid amplifications were done in XL-Gold Ultracompetent cells (Stratagene).

Mutant constructs pJAD.TM1, pJAD.TM2, pJAD.TM1&2 and pJAD.CTD, were generated using the InFusion<sup>®</sup> HD Cloning kit (Clontech), in combination with gBlock<sup>®</sup> gene fragments (IDT) containing the desired nucleotide changes (Supplementary Table 2). The primers and gBlock<sup>®</sup> gene fragments were designed in such a way to ensure the required 15 base pair homology needed for InFusion<sup>®</sup> cloning. To generate the linearized plasmid backbones, pJAD-S10 was amplified by inverse PCR using Phusion high-fidelity DNA polymerase (Thermo Fisher Scientific). The pJAD\_TM1, pJAD\_TM2 and pJAD\_CTD backbones were generated by using the TM1, TM2 and CTD primer sets respectively (Supplementary Table 3). The pJAD\_TM1&2 backbone was generated through use of the TM2 forward and TM1 reverse primers. PCR products were gel-purified using the NucleoSpin<sup>®</sup> Gel and PCR Clean-up kit (Macherey–Nagel). The linearised backbone was joined to its corresponding gBlock<sup>®</sup> insert. All cloning and plasmid amplifications were done in Stellar<sup>™</sup> competent cells (Clontech). Plasmid DNA was purified using the Genopure Plasmid Maxi kit (Roche Life Science) and introduced nucleotide changes verified by sequencing using the ABI PRISM BigDye Terminator Cycle Sequencing kit v3.1 (Applied Biosystems). Sequences were analysed using BioEdit (Hall, 1999).

### *Rescue of mutant viruses*

The recovery of mutant viruses was done using a plasmid only-based reverse genetics system described previously (Conradie et al., 2016). Monolayers of BSR-T7 cells in 6-well (9.5 cm<sup>2</sup>) tissue culture plates at 70% confluence were transfected with 500 ng of each dual plasmid (pJAD-S1-S8, pJAD-S2-S6, pJAD-S3-S7 and pJAD-S5-S9) and 250 ng of each single plasmid (pJAD-S4 and different mutant pJAD.S10 constructs) using 6.25 µl of Lipofectamine LTX (2.5 µl/ug of DNA) and 2.5 µl Plus<sup>TM</sup> reagent (1 µl/ug of DNA) (Invitrogen) each diluted in 125 µl of Opti-MEM<sup>®</sup> reduced serum medium. The rest of the protocol followed was as described by Conradie et al. (2016). The transfected cells were monitored for the appearance of CPE for 48 hours. If no CPE was observed, cells were passaged at least once. When sufficient CPE was observed, cells were harvested and dsRNA isolated using TRIzol<sup>®</sup> (Invitrogen). Total dsRNA was used for cDNA synthesis using the RevertAid H Minus First strand cDNA synthesis kit (Thermo Fisher Scientific). Seg-10 was selectively amplified by Phusion DNA polymerase using appropriate primers, PCR products were purified using a DNA Clean and Concentrator<sup>TM</sup> (Zymo Research) and sequenced. All transfections and amplifications that showed successful rescue were stored at 4°C until used for stock generation.

### *Antibodies*

Anti-NS3 serum was a kind gift from Dr Christiaan Potgieter. The serum was raised in rabbits at the animal facilities of Deltamune (Pty) Ltd with Ethic Approval number O-15-17 against a bacterially expressed and purified NS3\_TM1&2 protein. Rabbit anti-NS1 (Genscript) and anti-NS2 (Uitenweerde et al., 1995) antibodies were available. Mouse anti-NS1, anti-VP2 and anti-VP5 antibodies (Ingenasa, Spain) were also a gift from Dr Potgieter. Mouse anti-β-actin antibody was from Sigma Aldrich. Alexa Fluor<sup>TM</sup> 488 conjugated goat anti-rabbit (green) and Alexa Fluor<sup>TM</sup> 594 conjugated goat anti-mouse (red) secondary antibodies were from Thermo Fisher Scientific.

### *Immunoperoxidase monolayer assay*

Immunoperoxidase monolayer assays (IPMA) was done according to standard procedures (Wensvoort et al., 1988) for the detection of virus protein expression. Mammalian cell monolayers were infected with serial dilutions of the virus stocks and fixed with methanol:acetone (1:1) at 72 hours post infection (p.i.). Immunostaining was done with anti-NS2 sera diluted in blocking solution (1% tryptone and 0.05% Tween-20 [Sigma Aldrich] in 1X phosphate buffer saline [PBS]). Protein detection was via peroxidase-conjugated Protein A (Calbiochem®) and chromogen development using AEC reagent (Sigma Aldrich), or by anti-rabbit Alexa Fluor™ 488 and visualisation with a Zeiss Axiovert 200 Inverted Fluorescence microscope.

#### *Virus growth kinetics*

Confluent BSR cell monolayers seeded in 24-well (1.9 cm<sup>2</sup>) plates were infected, in triplicate, at an MOI of 0.1. At four time points post infection (12 h, 24 h, 48 h and 72 h p.i.) the culture medium was harvested (representing released virus fraction), and the remaining cells collected in fresh serum-free EMEM (representing cell-associated virus fraction). Samples were passed through a 22 G needle and virus titres in each fraction determined by endpoint dilution. Briefly, Vero cells were infected with 10-fold dilutions of each sample, fixed at 72 h p.i. and immunostained with anti-NS2 sera and Alexa Fluor® 488 for scoring purposes. Virus release was calculated as a percentage of the total virus yield, expressed as log<sub>10</sub> TCID<sub>50</sub>/ml. Each experiment was repeated at least once with independently prepared virus stocks.

#### *SDS-polyacrylamide gel electrophoresis (SDS-PAGE) and Western blot analysis*

Confluent BSR monolayers were infected with wild-type or mutant AHSV-4 at an MOI of 0.5-0.8. For whole cell lysates, the infected cells were harvested at 48 h p.i. in ice-cold hypotonic buffer (10 mM Tris [pH 8.0], 0.2 mM MgCl<sub>2</sub>, 1mg/ml Pepstatin and 0.7 mg/ml Pefabloc) and lysed with a 25G needle. For cell fractionation, following the harvesting of infected cells in hypotonic buffer at 60 h p.i. and lysing with a 25G needle, the soluble and insoluble fractions were subsequently collected by centrifugation at 16000 x g for 30 min. All protein samples were resolved by 12% SDS-PAGE. For Western blot analysis, the proteins from the unfixed gels were transferred to a Hybond nitrocellulose membrane (Amersham Biosciences) using standard

blotting techniques. Following blocking, the membranes were incubated with the anti-NS3 antibody. Peroxidase-conjugated protein A was used for detection.

#### *Cytotoxicity assay*

The CellTiter-Blue<sup>®</sup> cell viability assay was used according to the manufacturer's specifications. Briefly, confluent BSR monolayers seeded in 96-well plates were infected in quadruplicate at an MOI of 0.1. Uninfected cells and cells treated with 0.2% Triton X-100 (Sigma Aldrich) were included as viable and cell death controls. At select time points post infection the Resazurin reagent was added to the wells, followed by further incubation at 37°C. Fluorescence was measured after 3 hours using a SpectraMax Paradigm microplate reader (Molecular Devices USA) at the specified excitation/emission values (560<sub>Ex</sub>/590<sub>Em</sub>). Fluorescence values were compared to relevant controls and expressed as percentage cell viability.

#### *Immunofluorescence microscopy*

BSR cell monolayers were grown on sterile glass coverslips in 24-well plates, infected with wild-type or mutant AHSV-4 virus strains at an MOI of 0.5 and incubated at 37°C. Cells were fixed at 24 h p.i. with 4% PFA for 30 min at room temperature and permeabilized by treatment with 0.2% Triton X-100 in 1X PBS for 15 min. Cells were subsequently incubated in blocking solution (1% Tryptone and 0.05% Tween-20 in 1X PBS) at room temperature for 30 min followed by labelling with specific primary antibodies for at least 1 h. Cells were then washed three times with wash buffer (0.5% Tween-20 in PBS) and incubated for 1 h with the appropriate secondary antibodies. Cells were washed again, stained with DAPI (10 µg/ml) (Roche) for 10 min, washed once with 1X PBS and mounted onto glass slides using VECTASHIELD. For dual labelling the labelling was done sequentially, alternating between the appropriate primary and secondary antibodies. An additional blocking step, of 30 min at room temperature, was included before labelling with the second primary antibody. Slides were viewed either using a Zeiss LSM 510 Meta confocal microscope or a Zeiss LSM 880 with Airyscan. Colocalisation was calculated with the Coloc2 plugin in the FIJI software (Schindelin et al., 2012). Pearson's correlation coefficient above threshold values were determined of regions of interest.

### *Transmission electron microscopy (TEM)*

Confluent BSR monolayers seeded in six-well plates were infected at an MOI of 1. Mock infected control cells or AHSV infected cells were dislodged by scraping and concentrated into a loose pellet by low speed centrifugation. Approximately 0.5 µl of the pellet was transferred to a Leica membrane sample carrier. High-pressure freezing (HPF) was done with the Leica EMPACT2 HPF apparatus, followed by freeze-substitution (FS) in a Leica AFS2 for 72 hours. Cells were washed three times with 100% ethanol and embedded in LR White resin (SPI Supplies). Ultrathin (100 nm) sections were made with a Reichert Ultracut E microtome with a Diatome diamond knife. Samples for immunogold labelling, on copper-palladium grids, were blocked in potassium phosphate buffer (PPB) supplemented with 5% FBS and 0.05% Tween-20 for 30 min at room temperature. Grids were transferred to a drop of primary antibody diluted in blocking solution and incubated at room temperature for 2 hours before two consecutive washes for two min each in blocking solution, PPB and dH<sub>2</sub>O. Secondary labelling was done with an anti-rabbit 10 nm colloidal gold conjugate (SPI Supplies) diluted in blocking solution for 1 hour at room temperature followed by washing as above. Sample staining was in 1% aqueous uranyl acetate for 15 min and Reynold's lead citrate (Reynolds, 1963) for 3 min. Sample visualisation was done with a JEOL JEM-2100F field emission transmission electron microscope (FE-TEM).

## **Acknowledgements**

This work was supported by the University of Pretoria Institutional Research Theme (Grant A0V004), the Poliomyelitis Research Foundation (Grants 13/21 and 16/26) and the National Research Foundation of South Africa (Grant number 102209 and 116412). Graduate bursary support was received from Poliomyelitis Research Foundation and the University of Pretoria. We thank Flip Wege for technical assistance with cell culture and Dr Christiaan Potgieter for the use of their facilities, expertise and support in rescue of one of the mutant strains.

## References

- Beaton, A.R., Rodriguez, J., Reddy, Y.K., Roy, P., 2002. The membrane trafficking protein calpactin forms a complex with bluetongue virus protein NS3 and mediates virus release. *Proceedings of the National Academy of Sciences of the United States of America* 99, 13154-13159.
- Belhouchet, M., Mohd Jaafar, F., Firth, A.E., Grimes, J.M., Mertens, P.P., Attoui, H., 2011. Detection of a fourth orbivirus non-structural protein. *PloS one* 6, e25697.
- Bhattacharya, B., Celma, C.C., Roy, P., 2015. Influence of cellular trafficking pathway on bluetongue virus infection in ovine cells. *Viruses* 7, 2378-2403.
- Bhattacharya, B., Roy, P., 2008. Bluetongue virus outer capsid protein VP5 interacts with membrane lipid rafts via a SNARE domain. *Journal of virology* 82, 10600-10612.
- Blot, V., Perugi, F., Gay, B., Prevost, M.C., Briant, L., Tangy, F., Abriel, H., Staub, O., Dokhelar, M.C., Pique, C., 2004. Nedd4.1-mediated ubiquitination and subsequent recruitment of Tsg101 ensure HTLV-1 Gag trafficking towards the multivesicular body pathway prior to virus budding. *Journal of cell science* 117, 2357-2367.
- Bouamr, F., Melillo, J.A., Wang, M.Q., Nagashima, K., de Los Santos, M., Rein, A., Goff, S.P., 2003. PPPYVEPTAP motif is the late domain of human T-cell leukemia virus type 1 Gag and mediates its functional interaction with cellular proteins Nedd4 and Tsg101 [corrected]. *Journal of virology* 77, 11882-11895.
- Boyce, M., Celma, C.C., Roy, P., 2012. Bluetongue virus non-structural protein 1 is a positive regulator of viral protein synthesis. *Virology journal* 9, 178.

Bremer, C.W., Huismans, H., Van Dijk, A.A., 1990. Characterization and cloning of the African horsesickness virus genome. *The Journal of general virology* 71 ( Pt 4), 793-799.

Brown, D.A., London, E., 1998. Functions of lipid rafts in biological membranes. *Annual review of cell and developmental biology* 14, 111-136.

Buchholz, U.J., Finke, S., Conzelmann, K.-K., 1999. Generation of bovine respiratory syncytial virus (BRSV) from cDNA: BRSV NS2 is not essential for virus replication in tissue culture, and the human RSV leader region acts as a functional BRSV genome promoter. *Journal of virology* 73, 251-259.

Burkhardt, C., Sung, P.Y., Celma, C.C., Roy, P., 2014. Structural constraints in the packaging of bluetongue virus genomic segments. *The Journal of general virology* 95, 2240-2250.

Celma, C.C., Roy, P., 2009. A viral nonstructural protein regulates bluetongue virus trafficking and release. *Journal of virology* 83, 6806-6816.

Celma, C.C., Roy, P., 2011. Interaction of calpactin light chain (S100A10/p11) and a viral NS protein is essential for intracellular trafficking of nonenveloped bluetongue virus. *Journal of virology* 85, 4783-4791.

Chauveau, E., Doceul, V., Lara, E., Breard, E., Sailleau, C., Vidalain, P.-O., Meurs, E.F., Dabo, S., Schwartz-Cornil, I., Zientara, S., Vitour, D., 2013. NS3 of Bluetongue Virus Interferes with the Induction of Type I Interferon. *J. Virol.* 87, 8241-8246.

Conradie, A.M., Stassen, L., Huismans, H., Potgieter, C.A., Theron, J., 2016. Establishment of different plasmid only-based reverse genetics systems for the recovery of African horse sickness virus. *Virology* 499, 144-155.

Du Toit, R., 1944. The transmission of bluetongue and horse sickness by Culicoides. *Onderstepoort J Vet Sci Anim Ind* 19, 7-16.



Dunn, K.W., Kamocka, M.M., McDonald, J.H., 2011. A practical guide to evaluating colocalization in biological microscopy. *American journal of physiology. Cell physiology* 300, C723-742.

Erasmus, B., 1974. The pathogenesis of African horsesickness, *Equine Infectious Diseases*. Karger Publishers, pp. 1-11.

Evans, W.H., Graham, J.M., 1989. *Membrane structure and function*. Irl Press, Oxford, England.

Feenstra, F., van Gennip, R.G., Maris-Veldhuis, M., Verheij, E., van Rijn, P.A., 2014a. Bluetongue virus without NS3/NS3a expression is not virulent and protects against virulent bluetongue virus challenge. *The Journal of general virology* 95, 2019-2029.

Feenstra, F., van Gennip, R.G., van de Water, S.G., van Rijn, P.A., 2014b. RNA elements in open reading frames of the bluetongue virus genome are essential for virus replication. *PLoS One* 9, e92377.

Garrus, J.E., von Schwedler, U.K., Pornillos, O.W., Morham, S.G., Zavitz, K.H., Wang, H.E., Wettstein, D.A., Stray, K.M., Cote, M., Rich, R.L., Myszka, D.G., Sundquist, W.I., 2001. Tsg101 and the vacuolar protein sorting pathway are essential for HIV-1 budding. *Cell* 107, 55-65.

Hall, T.A., 1999. BioEdit: a user-friendly biological sequence alignment editor and analysis program for Windows 95/98/NT. *Nucl. Acids. Symp.* 41.

Han, Z., Harty, R.N., 2004. The NS3 protein of bluetongue virus exhibits viroporin-like properties. *The Journal of biological chemistry* 279, 43092-43097.

Ingham, R.J., Gish, G., Pawson, T., 2004. The Nedd4 family of E3 ubiquitin ligases: functional diversity within a common modular architecture. *Oncogene* 23, 1972-1984.

Lodish, H., Berk, A., Kaiser, C., Krieger, M., Scott, M., Bretscher, A., Ploegh, H., 2004. Moving proteins into membranes and organelles. Vesicular traffic, Secretion, and Endocytosis., 5th ed. W. H. Freeman and Company.

Lodish, H., Berk, A., Zipursky, S., Matsudaira, P., Baltimore, D., Darnell, J., 2000. Overview of the secretory pathway WH Freeman and Company.

Macara, I.G., 2001. Transport into and out of the nucleus. *Microbiology and molecular biology reviews* 65, 570-594.

Manole, V., Laurinmaki, P., Van Wyngaardt, W., Potgieter, C.A., Wright, I.M., Venter, G.J., van Dijk, A.A., Sewell, B.T., Butcher, S.J., 2012. Structural Insight into African Horsesickness Virus Infection. *J. Virol.* 86, 7858-7866.

Martin-Serrano, J., Eastman, S.W., Chung, W., Bieniasz, P.D., 2005. HECT ubiquitin ligases link viral and cellular PPXY motifs to the vacuolar protein-sorting pathway. *The Journal of cell biology* 168, 89-101.

Meiring, T.L., Huisman, H., van Staden, V., 2009. Genome segment reassortment identifies non-structural protein NS3 as a key protein in African horsesickness virus release and alteration of membrane permeability. *Archives of virology* 154, 263-271.

Mellor, P.S., Hamblin, C., 2004. African horse sickness. *Vet Res* 35, 445-466.

Owens, R.J., Limn, C., Roy, P., 2004. Role of an arbovirus nonstructural protein in cellular pathogenesis and virus release. *Journal of virology* 78, 6649-6656.

Parent, L.J., Bennett, R.P., Craven, R.C., Nelle, T.D., Krishna, N.K., Bowzard, J.B., Wilson, C.B., Puffer, B.A., Montelaro, R.C., Wills, J.W., 1995. Positionally independent and exchangeable late budding functions

of the Rous sarcoma virus and human immunodeficiency virus Gag proteins. *Journal of virology* 69, 5455-5460.

Parr, R.D., Storey, S.M., Mitchell, D.M., McIntosh, A.L., Zhou, M., Mir, K.D., Ball, J.M., 2006. The rotavirus enterotoxin NSP4 directly interacts with the caveolar structural protein caveolin-1. *Journal of virology* 80, 2842-2854.

Ratinier, M., Caporale, M., Golder, M., Franzoni, G., Allan, K., Nunes, S.F., Armezzani, A., Bayoumy, A., Rixon, F., Shaw, A., Palmarini, M., 2011. Identification and characterization of a novel non-structural protein of bluetongue virus. *PLoS pathogens* 7, e1002477.

Reynolds, E.S., 1963. The use of lead citrate at high pH as an electron-opaque stain in electron microscopy. *The Journal of cell biology* 17, 208-212.

Schindelin, J., Arganda-Carreras, I., Frise, E., Kaynig, V., Longair, M., Pietzsch, T., Preibisch, S., Rueden, C., Saalfeld, S., Schmid, B., 2012. Fiji: an open-source platform for biological-image analysis. *Nature methods* 9, 676.

Sealfon, R.S., Lin, M.F., Jungreis, I., Wolf, M.Y., Kellis, M., Sabeti, P.C., 2015. FRESCo: finding regions of excess synonymous constraint in diverse viruses. *Genome biology* 16, 38.

Stassen, L., Huismans, H., Theron, J., 2011. Membrane permeabilization of the African horse sickness virus VP5 protein is mediated by two N-terminal amphipathic alpha-helices. *Arch Virol* 156, 711-715.

Stassen, L., Huismans, H., Theron, J., 2012. African horse sickness virus induces apoptosis in cultured mammalian cells. *Virus Res* 163, 385-389.

Stewart, M., Hardy, A., Barry, G., Pinto, R.M., Caporale, M., Melzi, E., Hughes, J., Taggart, A., Janowicz, A., Varela, M., Ratnier, M., Palmarini, M., 2015. Characterization of a second open reading frame in genome segment 10 of bluetongue virus. *The Journal of general virology* 96, 3280-3293.

Strack, B., Calistri, A., Accola, M.A., Palu, G., Gottlinger, H.G., 2000. A role for ubiquitin ligase recruitment in retrovirus release. *Proceedings of the National Academy of Sciences of the United States of America* 97, 13063-13068.

Strack, B., Calistri, A., Gottlinger, H.G., 2002. Late assembly domain function can exhibit context dependence and involves ubiquitin residues implicated in endocytosis. *Journal of virology* 76, 5472-5479.

Uitenweerde, J.M., Theron, J., Stoltz, M.A., Huismans, H., 1995. The Multimeric Nonstructural NS2 Proteins of Bluetongue Virus, African Horsesickness Virus, and Epizootic Hemorrhagic Disease Virus Differ in Their Single-Stranded RNA-Binding Ability. *Virology* 209, 624-632.

Usami, Y., Popov, S., Popova, E., Inoue, M., Weissenhorn, W., H, G.G., 2009. The ESCRT pathway and HIV-1 budding. *Biochemical Society transactions* 37, 181-184.

van de Water, S.G., van Gennip, R.G., Potgieter, C.A., Wright, I.M., van Rijn, P.A., 2015. VP2 Exchange and NS3/NS3a Deletion in African Horse Sickness Virus (AHSV) in Development of Disabled Infectious Single Animal Vaccine Candidates for AHSV. *Journal of virology* 89, 8764-8772.

Van Gennip, R.G.P., Van de Water, S.G., Van Rijn, P.A., 2014. Bluetongue Virus Nonstructural Protein NS3/NS3a Is Not Essential for Virus Replication. *PloS one* 9.

van Niekerk, M., Smit, C.C., Fick, W.C., van Staden, V., Huismans, H., 2001. Membrane association of African horsesickness virus nonstructural protein NS3 determines its cytotoxicity. *Virology* 279, 499-508.

van Rijn, P.A., Maris-Veldhuis, M.A., Potgieter, C.A., van Gennip, R.G.P., 2018. African horse sickness virus (AHSV) with a deletion of 77 amino acids in NS3/NS3a protein is not virulent and a safe promising AHS Disabled Infectious Single Animal (DISA) vaccine platform. *Vaccine* 36, 1925-1933.

van Staden, V., Huismans, H., 1991. A comparison of the genes which encode non-structural protein NS3 of different orbiviruses. *The Journal of general virology* 72 ( Pt 5), 1073-1079.

van Staden, V., Smit, C.C., Stoltz, M.A., Maree, F.F., Huismans, H., 1998. Characterization of two African horse sickness virus nonstructural proteins, NS1 and NS3. *Arch Virol Suppl* 14, 251-258.

van Staden, V., Stoltz, M.A., Huismans, H., 1995. Expression of nonstructural protein NS3 of African horsesickness virus (AHSV): evidence for a cytotoxic effect of NS3 in insect cells, and characterization of the gene products in AHSV infected Vero cells. *Arch Virol* 140, 289-306.

Vana, M.L., Tang, Y., Chen, A., Medina, G., Carter, C., Leis, J., 2004. Role of Nedd4 and ubiquitination of Rous sarcoma virus Gag in budding of virus-like particles from cells. *Journal of virology* 78, 13943-13953.

Venter, E., van der Merwe, C.F., Buys, A.V., Huismans, H., van Staden, V., 2014. Comparative ultrastructural characterisation of African horse sickness virus-infected mammalian and insect cells reveals novel potential virus release mechanism from insect cells. *J. Gen. Virol.* 95, 642-651.

Venter, G., Wright, I., Van Der Linde, T., Paweska, J., 2009. The oral susceptibility of South African field populations of *Culicoides* to African horse sickness virus. *Medical and veterinary entomology* 23, 367-378.

Vermaak, E., Theron, J., 2015. Virus uncoating is required for apoptosis induction in cultured mammalian cells infected with African horse sickness virus. *The Journal of general virology* 96, 1811-1820.

VerPlank, L., Bouamr, F., LaGrassa, T.J., Agresta, B., Kikonyogo, A., Leis, J., Carter, C.A., 2001. Tsg101, a homologue of ubiquitin-conjugating (E2) enzymes, binds the L domain in HIV type 1 Pr55(Gag). *Proceedings of the National Academy of Sciences of the United States of America* 98, 7724-7729.

Wang, R., Brattain, M.G., 2007. The maximal size of protein to diffuse through the nuclear pore is larger than 60 kDa. *FEBS letters* 581, 3164-3170.

Wensvoort, G., Terpstra, C., Bloemraad, M., 1988. Detection of antibodies against African swine fever virus using infected monolayers and monoclonal antibodies. *The Veterinary record* 122, 536-539.

Wirblich, C., Bhattacharya, B., Roy, P., 2006. Nonstructural protein 3 of bluetongue virus assists virus release by recruiting ESCRT-I protein Tsg101. *Journal of virology* 80, 460-473.

Wu, X., Chen, S.Y., Iwata, H., Compans, R.W., Roy, P., 1992. Multiple glycoproteins synthesized by the smallest RNA segment (S10) of bluetongue virus. *J Virol* 66, 7104-7112.

Zhang, X., Boyce, M., Bhattacharya, B., Zhang, X., Schein, S., Roy, P., Zhou, Z.H., 2010. Bluetongue virus coat protein VP2 contains sialic acid-binding domains, and VP5 resembles enveloped virus fusion proteins. *Proceedings of the National Academy of Sciences of the United States of America* 107, 6292-6297.

Zientara, S., Weyer, C.T., Lecollinet, S., 2015. African horse sickness. *Rev Sci Tech* 34, 315-327.

Zwart, L., Potgieter, C.A., Clift, S.J., van Staden, V., 2015. Characterising Non-Structural Protein NS4 of African Horse Sickness Virus. *PloS one* 10, e0124281.

## Figure legends:

**Fig. 1.** A) Schematic overview of the wildtype AHSV-4 NS3 protein and the nine proposed mutant constructs. The position of the NS3 and NS3A start codons, L-domain, transmembrane domains and C-terminal domain are indicated. Specific amino acid changes are shown and highlighted by a \*; solid lines and boxes represent putatively translated sequences; dashed lines represent the expected absence of translation or deletions. B) Expression of wild-type and mutant NS3/A proteins. Infected BSR cells were harvested, lysed and assayed for the presence of NS3/A in whole cell lysates or soluble and insoluble fractions, labelling with an anti-NS3 antibody and an anti- $\beta$ -actin antibody. (-) represents mock-infected cells; (+) represents positive control.

**Fig. 2.** A) Plaque assays of all virus strains. Three days following infection of BSR cell monolayers, the samples were stained with 0.1% MTT. Mock infected cells were included as control. B) IPMA of Vero cells infected with tenfold dilutions of the wild-type and mutant AHSV-4 strains. Cells were fixed with methanol:acetone (1:1) at 72 h .p.i. and immunostained with an anti-NS2 antibody and peroxidase-conjugated Protein A. Visualisation was done after the addition of AEC reagent and sufficient chromogen development. Mock infected cells were included as control. Scale bars represent 200  $\mu$ m.

**Fig. 3.** Virus release and cell viability over 72 hours following infection of BSR cells for wild-type and all mutant virus strains. A) Percentage virus released from infected cells (average released titre/average total yield\*100). Titrations were done in quadruplicate for all three biological repeats at all three time points. B) Percentage viable cells remaining as infection proceeds. At least four biological repeats were included per sample per time point. Standard deviation indicated for all samples, as well as any statistically significant differences to the wild-type virus, as calculated by the paired Student's t test (\*\*  $p < 0.05$ ; +  $p < 0.1$ ).

**Fig. 4.** Intracellular distribution of NS3/A within AHSV-4 infected mammalian cells. BSR monolayers were infected with wild-type or mutant virus strains and fixed at 24 h p.i. Mock infected cells were included as

control. AHSV4\_WT, AHSV4\_LD1, AHSV4\_LD2 and AHSV\_CTD show perinuclear and membrane localisation of NS3/A. AHSV4\_TM1, AHSV4\_TM2 and AHSV4\_TM1&2 show altered NS3/A localisation to the cell nucleus and lack of membrane binding. NS3/A was detected with an anti-NS3 antibody (rabbit) and Alexa Fluor<sup>TM</sup> 488 conjugated goat anti-rabbit secondary antibody (green). Nuclei were stained with DAPI (blue). Scale bars represent 10  $\mu$ m.

**Fig. 5.** TEM micrographs depicting NS3/A localisation in mammalian cells. BSR monolayers were infected with the wild-type or mutant viruses. Ultrathin sections were labelled with anti-NS3 antibody (rabbit) and a gold conjugated anti-rabbit secondary antibody. In wild-type infected cells, the NS3 protein localises to the plasma membrane and at perinuclear vesicles within the cytoplasm. In cells infected with AHSV4\_TM1, the mutant NS3 protein localises to nuclear foci and NS1 tubules. Insert – TEM micrograph depicting labelling of an anti-NS1 antibody (rabbit) to NS1 tubules in BSR cells infected with AHSV4\_TM1. CYT – cytoplasm; PM – plasma membrane; NM – nuclear membrane; T- tubules; arrows indicate areas of positive labelling. Scale bar represents 200 nm.

**Fig. 6.** Intracellular localisation of NS3/A and NS1 within AHSV-4 infected mammalian cells. BSR monolayers were infected with wild-type or transmembrane mutant AHSV-4 virus strains and fixed at 24 h p.i. While no association could be detected for the wild-type virus, the transmembrane mutant's NS3 signal only appears as tubules in areas with simultaneous NS1 localisation (arrows); otherwise NS3 appears as foci (box) or diffuse. NS3 was detected with an anti-NS3 antibody (rabbit) and Alexa Fluor<sup>TM</sup> 488 conjugated goat anti-rabbit secondary antibody (green). NS1 was detected with an anti-NS1 antibody (mouse) and Alexa Fluor<sup>TM</sup> 594 conjugated goat anti-mouse secondary antibody (red). Nuclei were stained with DAPI (blue). Scale bars represent 10  $\mu$ m.

**Fig. 7.** Intracellular distribution of VP2 within AHSV-4 infected mammalian cells. BSR monolayers were infected with wild-type and mutant AHSV-4 virus strains and fixed at 24 h p.i. Mock infected cells were included as control. AHSV4\_WT and AHSV4\_STR2 shows small foci throughout the cytoplasm.



AHSV4\_LD1 and AHSV4\_LD2 shows prevalent membrane binding. AHSV4\_TM1, AHSV4\_TM2 and AHSV4\_TM1&2 show larger foci throughout the cytoplasm, while AHSV4\_CTD shows both cytoplasmic foci, with some membrane localisation. VP2 was detected with an anti-VP2 antibody (mouse) and Alexa Fluor™ 594 conjugated goat anti-mouse secondary antibody (red). Nuclei were stained with DAPI (blue). Arrows indicate some areas with membrane association. Scale bars represent 10 µm.

**Fig. 8.** TEM micrographs depicting virus particle localisation in mammalian cells. BSR monolayers were infected with wild-type or mutant viruses. AHSV4\_WT, AHSV4\_STR2, AHSV4\_LD1 and AHSV4\_LD2 showed prevalently small cytoplasmic virus aggregates. AHSV4\_TM1, AHSV4\_TM2, AHSV4\_TM1&2 and AHSV4\_CTD showed large cytoplasmic virus aggregates. Bottom right micrograph represents the mutant phenotype of virus particles tethered to the plasma membrane of cells infected with AHSV4\_LD2. CYT – cytoplasm; V – virus particles; PM – plasma membrane; scale bar represents 1 µm.

**Fig. 9.** Assessing VIBs within AHSV-4 infected mammalian cells. Top left micrograph illustrates the presence of virus aggregates adjacent to VIBs (indicated by arrows) in cells infected with AHSV4\_CTD. The remaining two images represent MIPs of BSR monolayers infected with AHSV4\_WT and AHSV4\_TM2. Cells were fixed at 24 h p.i. and NS2 was detected with an anti-NS2 antibody (rabbit) and Alexa Fluor™ 488 conjugated goat anti-rabbit secondary antibody (green). Nuclei were stained with DAPI (blue). Stacked bar graph represents the percentage VIBs present in each size category at 24 h p.i. MIPs of each virus was analysed with ImageJ, identifying 20 cells per virus and calculating the µm<sup>2</sup> size of each VIB. AHSV4\_WT and AHSV4\_STR2 showed the highest proportion of small VIBs; followed by AHSV4\_LD1 and AHSV4\_LD2 that appeared more intermediate; and AHSV4\_TM1, AHSV4\_TM2, AHSV4\_TM1&2 and AHSV4\_CTD showing the highest proportion of large VIBs.

Figure 1

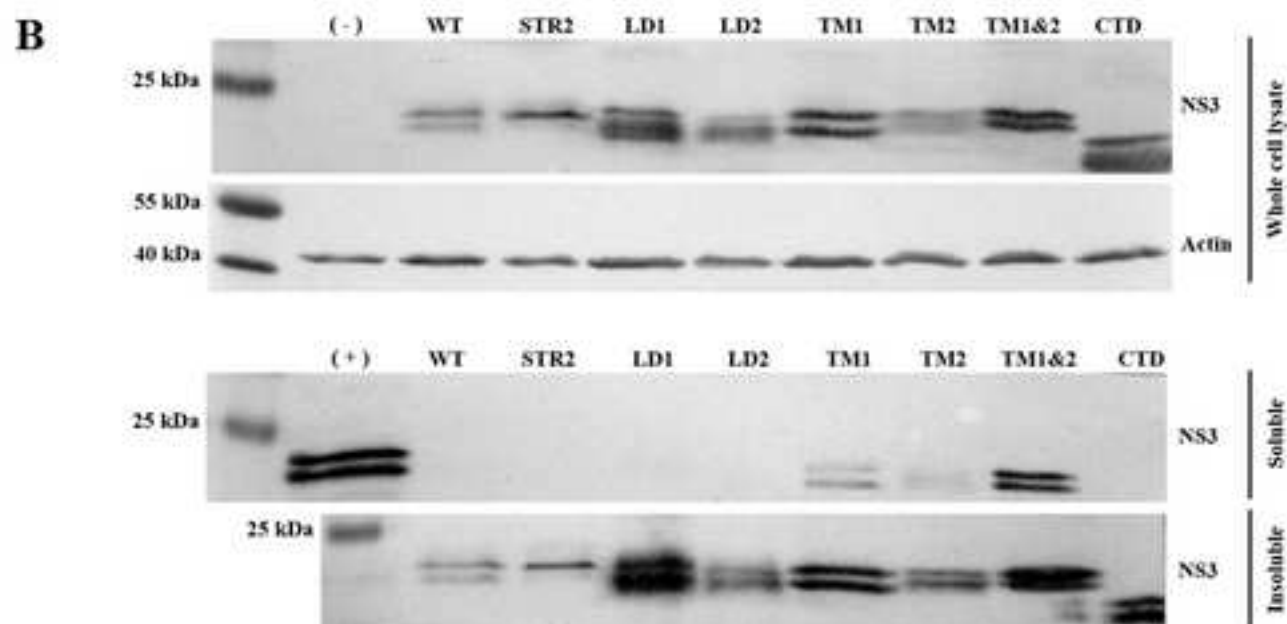
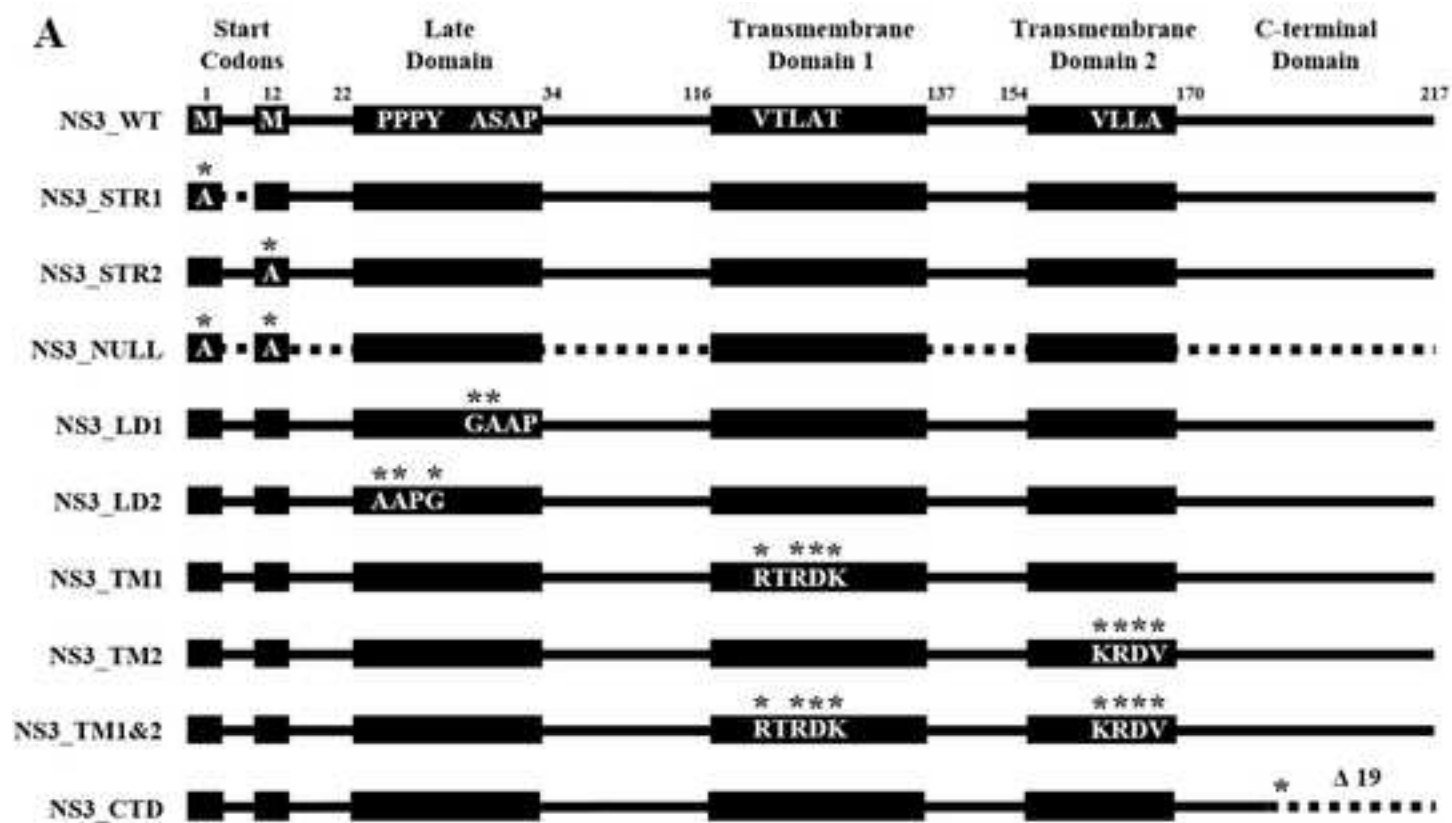


Figure 2

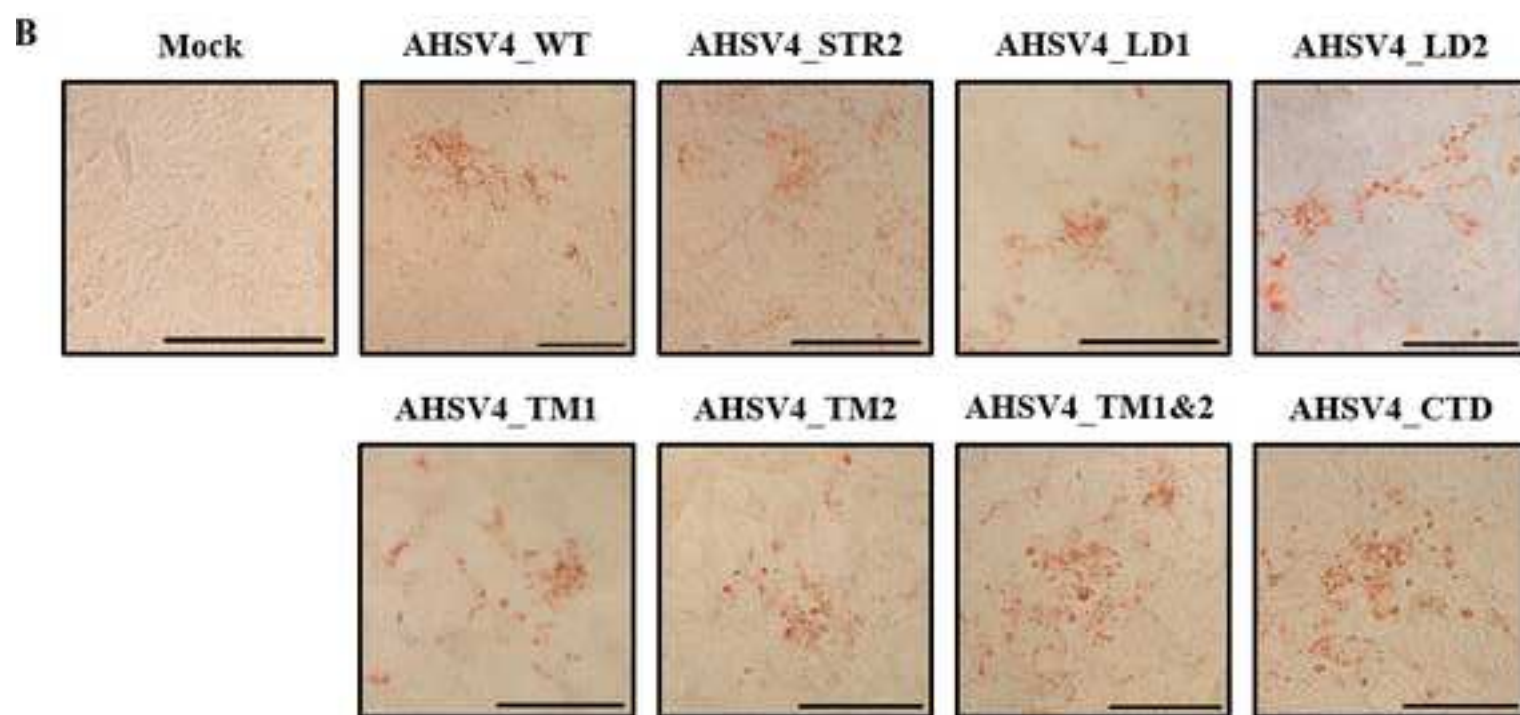
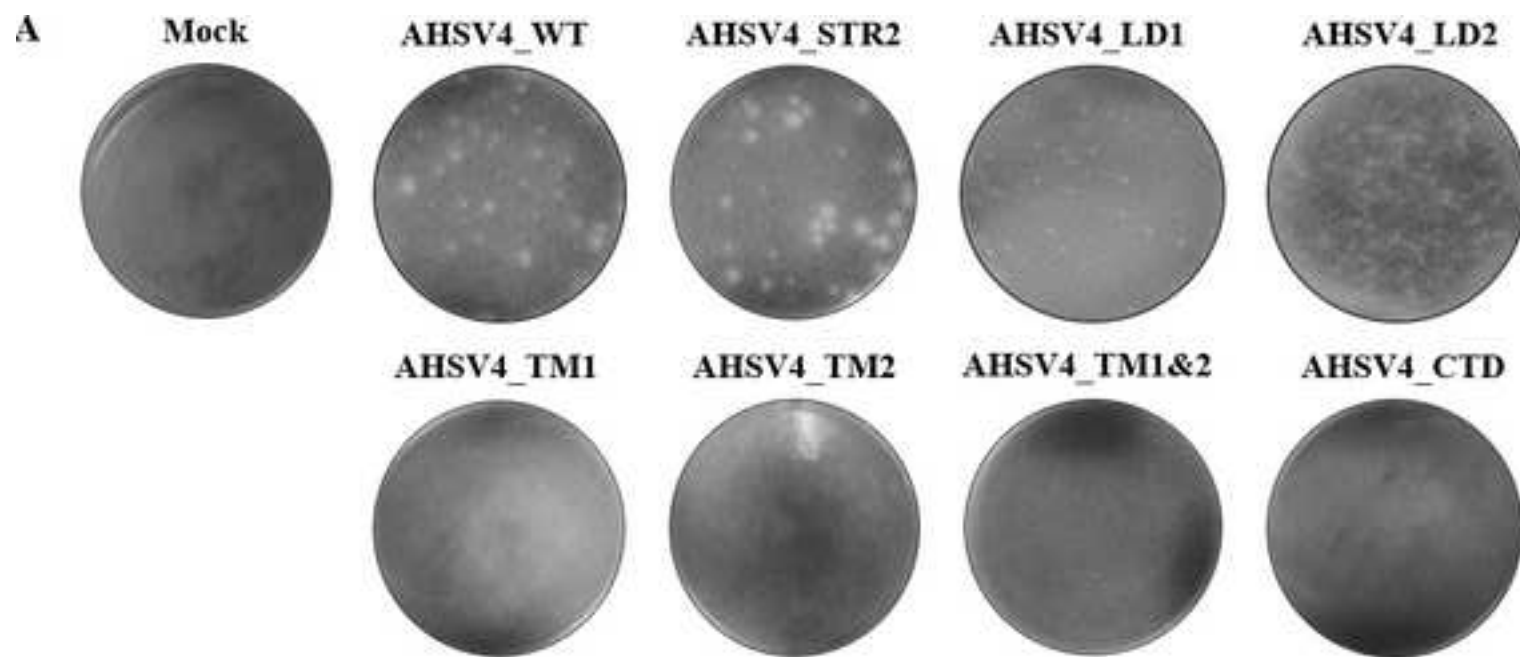


Figure 3

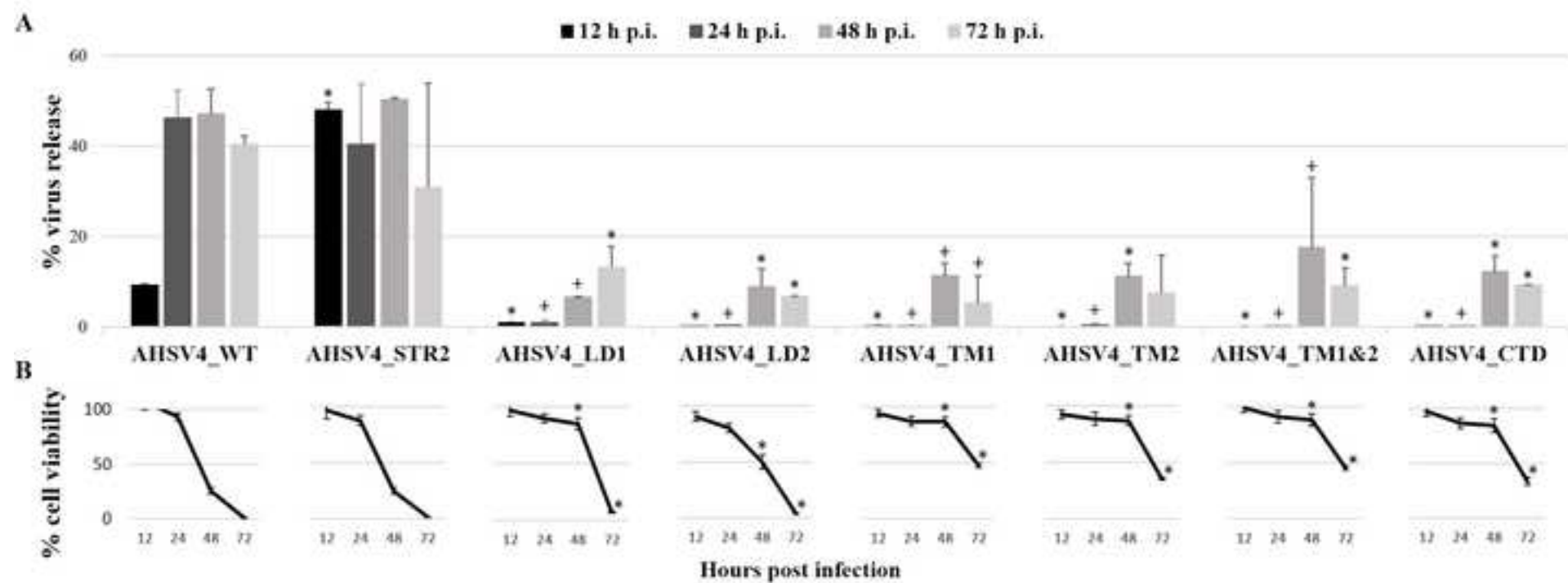


Figure 4

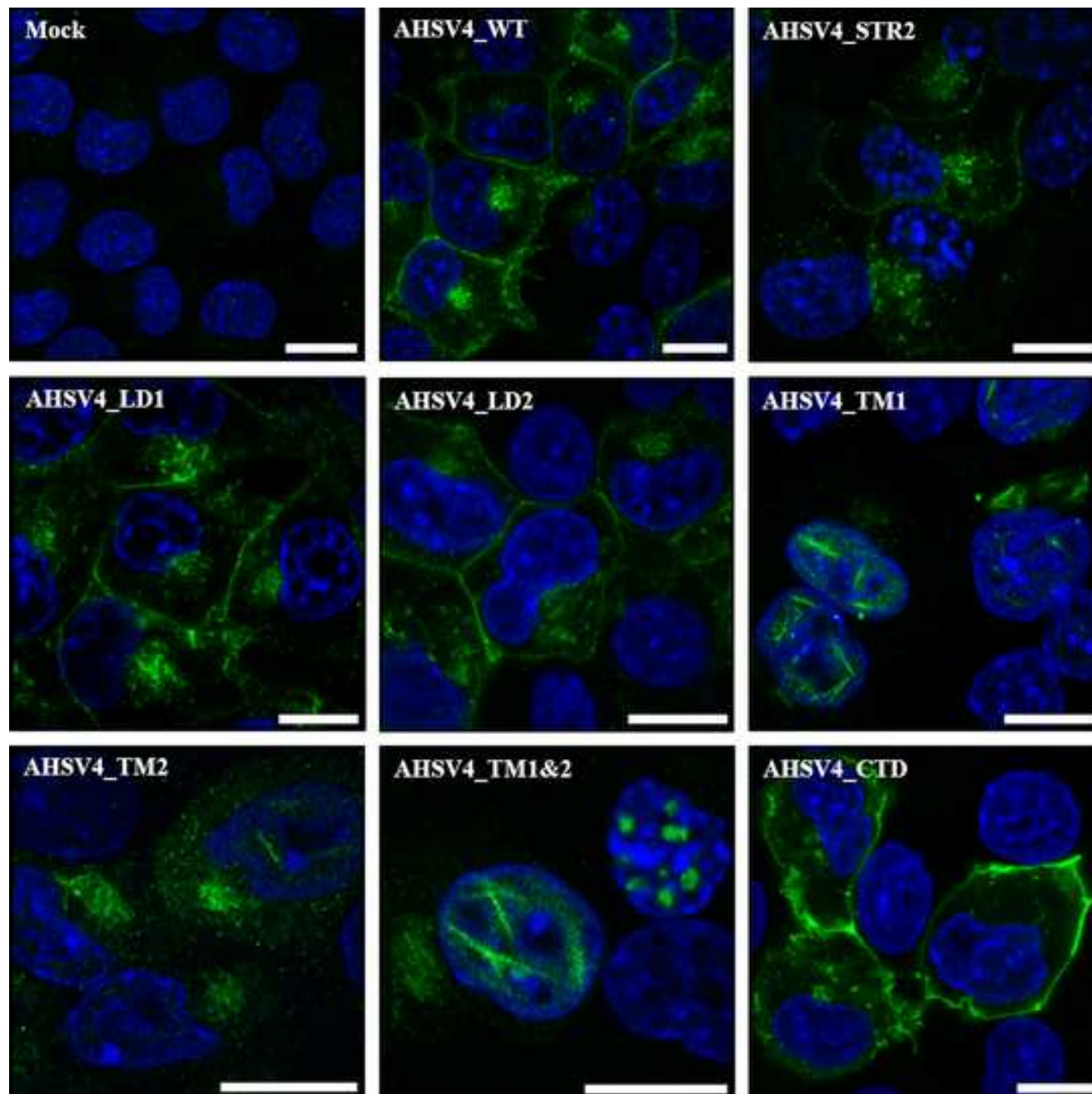




Figure 5

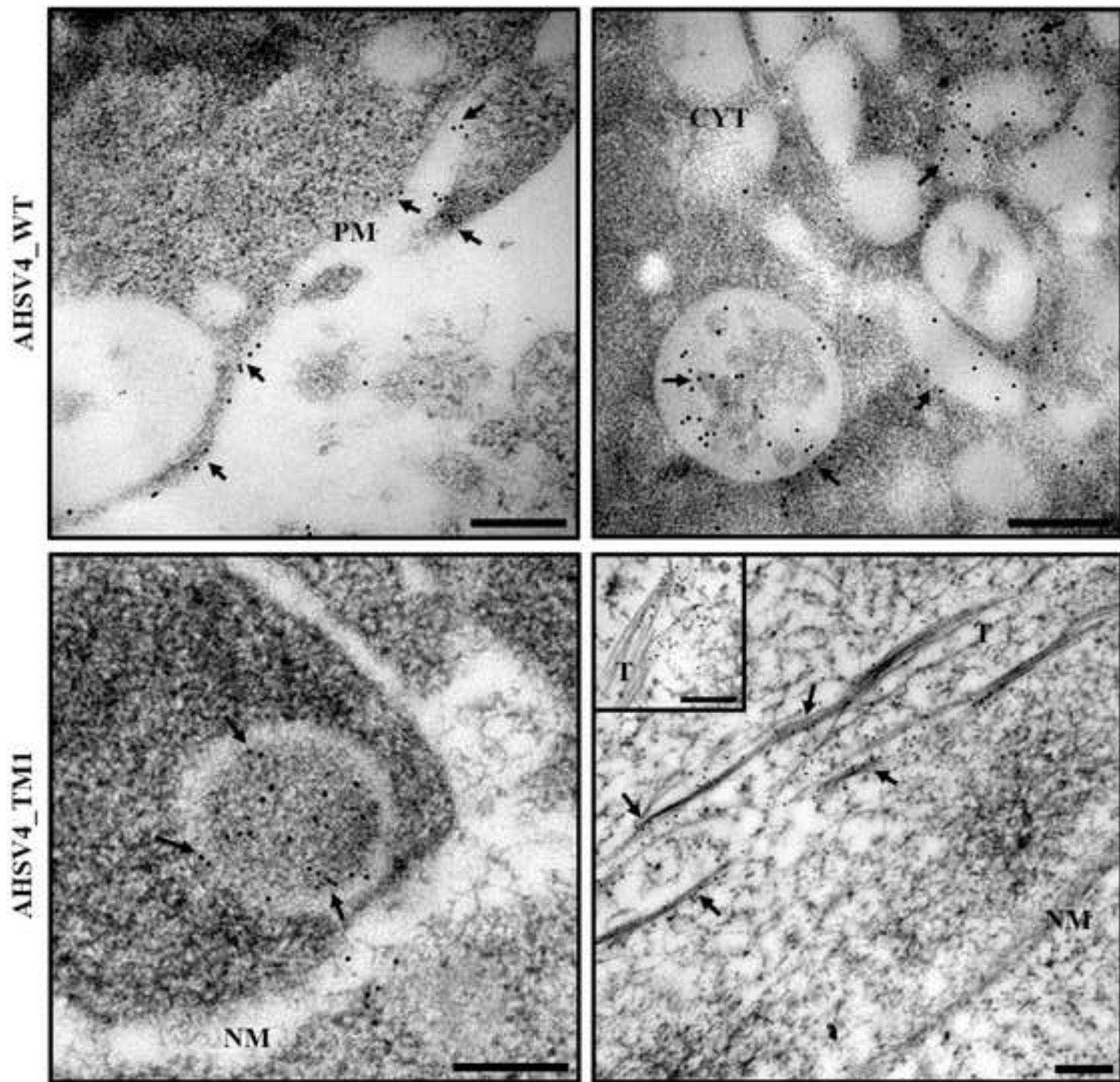


Figure 6

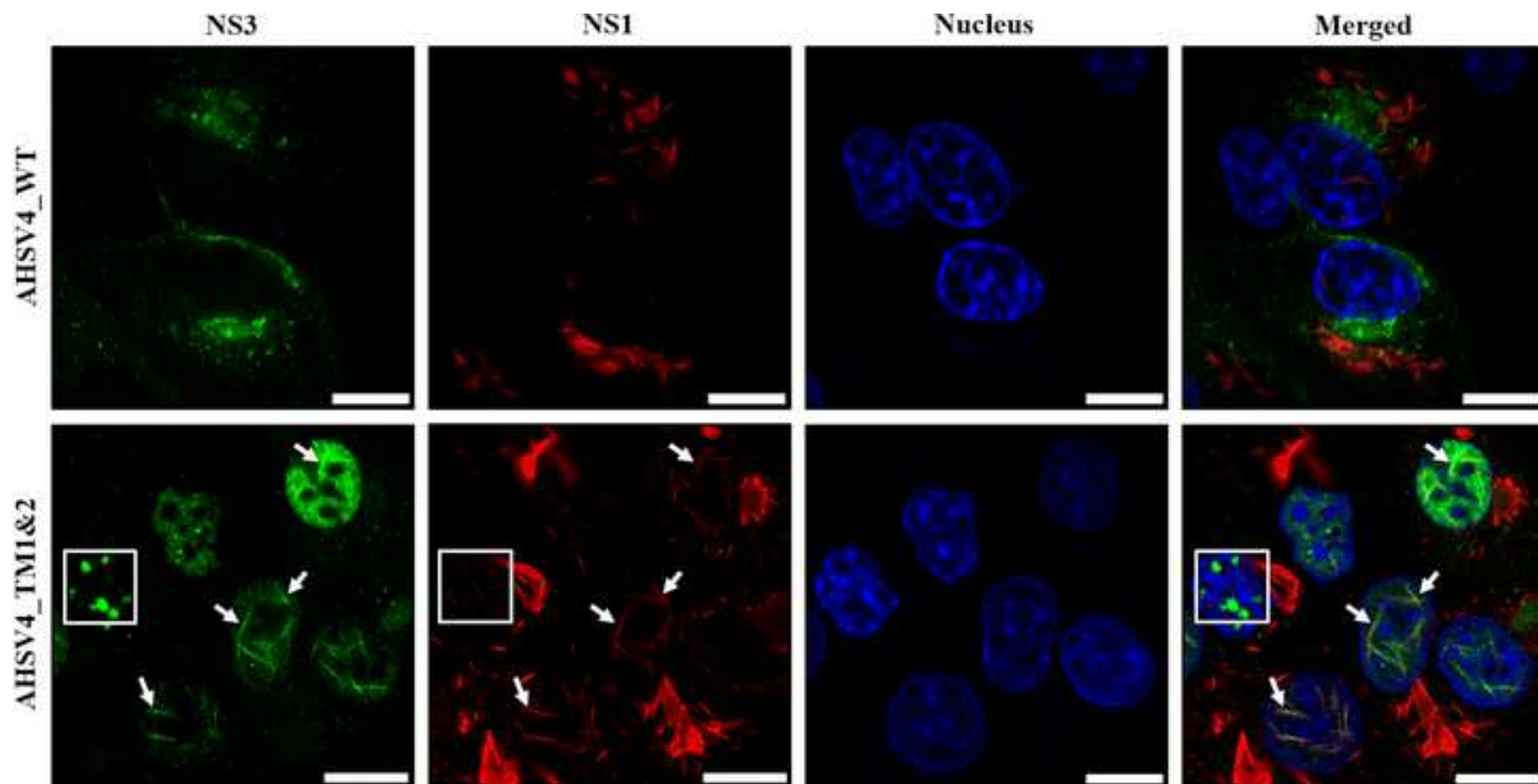


Figure 7

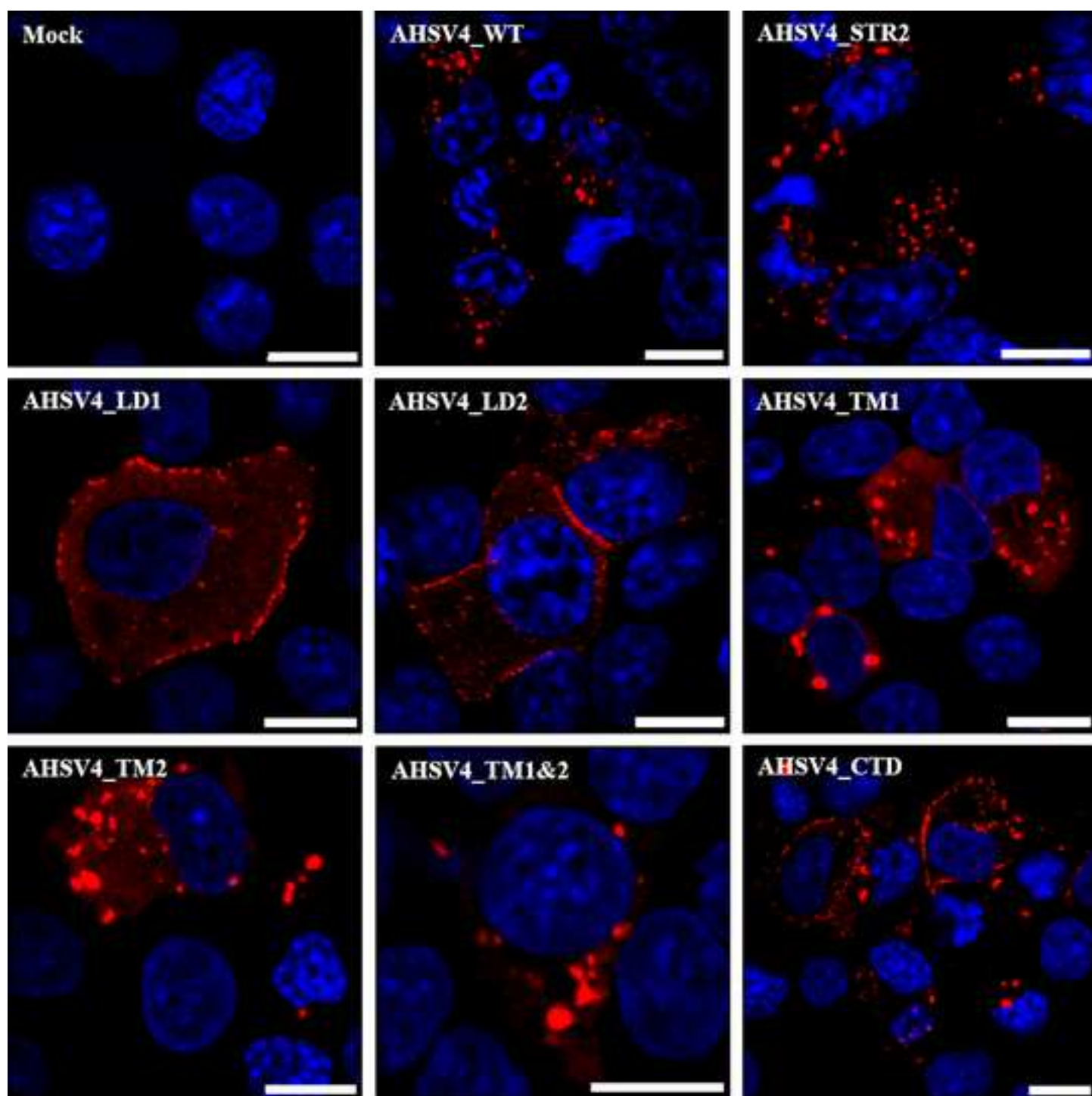




Figure 8

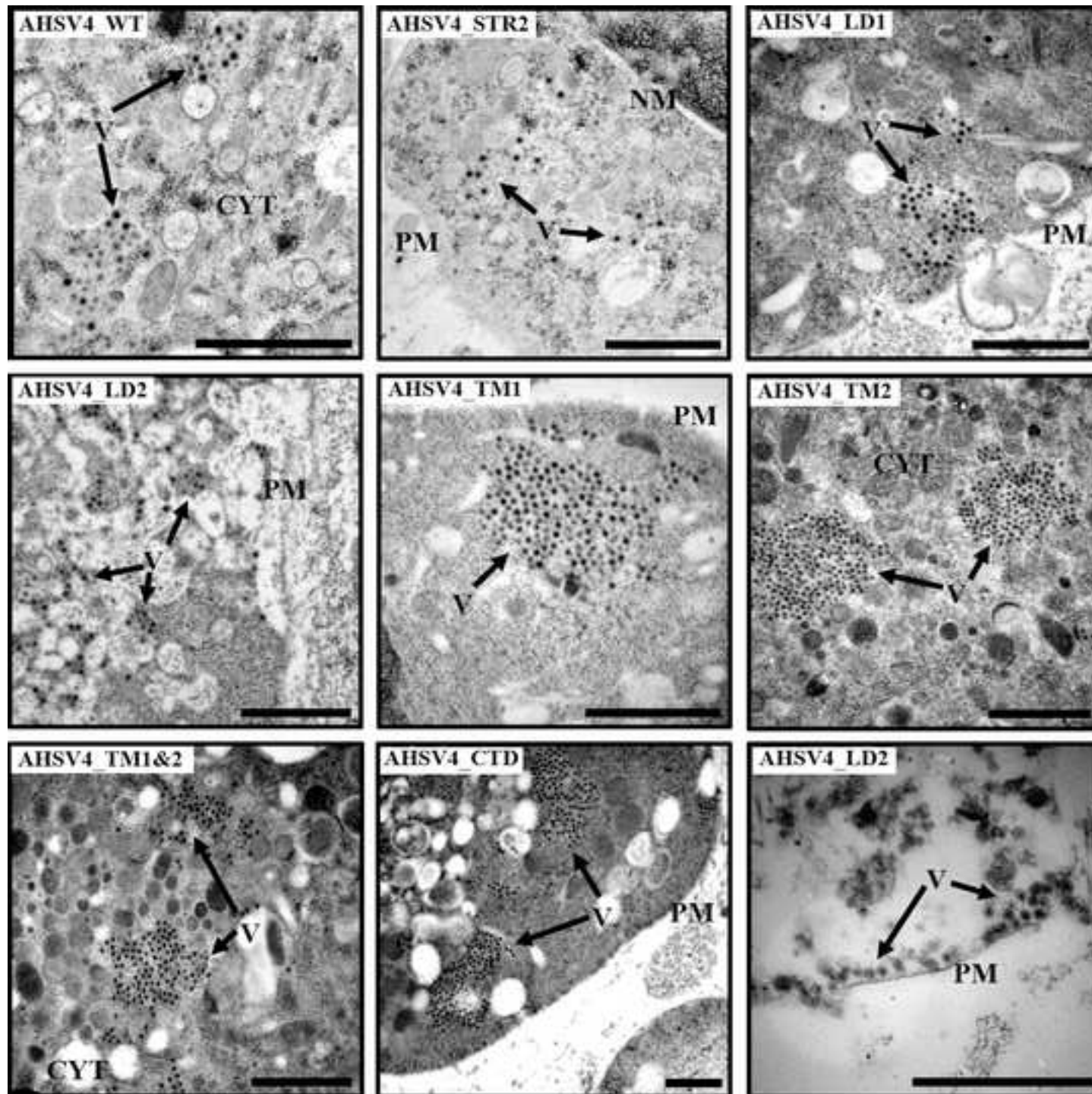


Figure 9

